Chemical Engineering Journal 433 (2022) 134442

Contents lists available at ScienceDirect

Chemical Engineering Journal

journal homepage: www.elsevier.com/locate/cej

Novel calixarene-based porous organic polymers with superfast removal rate and ultrahigh adsorption capacity for selective separation of cationic dyes

Shiyuan Zhou [a,1], Liujun Jin [a,1], Peiyang Gu [a], Lechen Tian [a], Najun Li [a], Dongyun Chen [a], Antonio Marcomini [b], Qingfeng Xu [a], Jianmei Lu [a,*]

[a] College of Chemistry, Chemical Engineering and Materials Science, Collaborative Innovation Center of Suzhou Nano Science and Technology, Soochow University, Suzhou, Jiangsu 215123, China

[b] Department of Environmental Sciences, Informatics and Statistics, University Ca' Foscari Venice, I-30170 Venice, Italy

ARTICLE INFO

Keywords:
Porous organic polymers
Superfast adsorption rate
Ultrahigh adsorption capacity
Selective adsorption
Cationic dyes

ABSTRACT

Exploring novel porous adsorbents for efficient water purification is a significant and urgent task. Two novel calixarene-based porous organic polymers (POPs) namely POP-8F and POP-10F were synthesized via a simple and mild reaction using octafluoronaphthalene and decafluorobiphenyl as the crosslinker. The Fourier transform infrared spectrometer, solid-state ^{13}C NMR spectra prove the successful construction of the POPs, and thermal gravimetric analyzer curves demonstrate the good thermal stabilities. Combining the advantages of porous structures, abundant adsorption sites and electronegative natures, both POP-8F and POP-10F exhibit extraordinary adsorption capacities and rates towards cationic dyes including Rhodamine B (RhB), methylene blue (MB) and crystal violet (CV). Especially for RhB, the removal efficiency can reach nearly 99 % within 4 min and the pseudo-second-order rate constant of POP-8F is 0.04386 g mg^{-1} min^{-1}. Notably, the maximum adsorption capacity of POP-8F towards RhB is 2433 mg g^{-1}, surpassing all the previously reported porous adsorbents including covalent organic frameworks, metal organic frameworks, POPs, biomass adsorbents, activated carbons, etc. In addition, both POP-8F and POP-10F can selectively adsorb cationic dyes among the mixtures of cationic dyes and anionic dyes. More importantly, the calixarene-based POPs can efficiently remove cationic dyes through a simple column filtration and exhibit excellent reusability properties. All the above characteristics make POP-8F and POP-10F excellent porous adsorbents for water pollutant treatment and purification.

1. Introduction

The rapid development of chemical industries over the past decades has fabricated massive chemical pollutants, which are hard to be naturally degraded and have caused global contamination to the surrounding water, seriously threatening the dwelling environment and human health [1–5]. Among these chemical pollutants, the organic dyes are the most frequent and harmful ones owing to the broad applications in the paper, textile, cosmetic, wood, paint industries and the irreversible damage to the genital system of humans, even increasing the probability of suffering from cancers [6–9]. Therefore, water purification, especially efficient removal of dyes has become an urgent topic, which needs the joint efforts of the scientists all around the world. Currently, several removal approaches including photocatalysis [10–12], membrane filtration[13], oxidative degradation [14], biological treatment [15,16] and adsorption [17–19] have been adopted. Among them, adsorption has attracted growing worldwide attention and recognition owing to the unique advantages including high removal efficiency, low cost, simplicity and convenience [19]. The most common adsorbents are porous materials such as covalent organic frameworks (COFs) [20], metal–organic frameworks (MOFs) [21], activated carbons [22], biocomposite microspheres [23,24], etc. However, the disadvantages including difficulties of synthesis, high cost, instability, low adsorption rate and capacity have severely limited the development of the above adsorbents. Consequently, exploring novel porous adsorbents with the superiorities including simplicity of preparation, low cost, high

* Corresponding author.
E-mail address: lujm@suda.edu.cn (J. Lu).
[1] Shiyuan Zhou and Liujin Jin contributed equally to this work.

https://doi.org/10.1016/j.cej.2021.134442
Received 8 October 2021; Received in revised form 28 December 2021; Accepted 29 December 2021
Available online 1 January 2022

adsorption rate and capacity, selectivity and reusability should be a preferential research area.

Porous organic polymers (POPs), a new kind of porous adsorbents synthesized only using organic building blocks and connected via strong covalent bonds, with high specific surface areas, adjustable porosities, tunable structures, excellent stabilities, diverse functionalities and abundant active sites, have attracted increasing attentions and exhibited infinite potentiality [25–29]. Because of the multiple selections of building blocks and polymerization reactions, the modularity of POPs is very high and the porosities, structures and functional groups of POPs can be conveniently designed and adjusted [30], thus the POPs are capable to be used for various applications including photocatalysis [31], fluorescence sensing [32], energy storage [33], adsorption [34–36], etc. The efficient removal of organic dyes is an essential hotspot in the application of POPs-based adsorbents, and numerous POPs with different building blocks have been designed and synthesized in the last several years [37].

Calix[n]arene derivatives, synthesized through the condensation of phenols and formaldehydes derivatives, with the cuplike shapes, are one of the most burgeoning building blocks of POPs [38–40]. Currently, a variety of calix[n]arene-based POPs have been designed and prepared for the porous adsorbents of heavy metals, iodine [41,42], phenols [43], pesticides [44], perfluoroalkyl substances [45] and organic dyes [46,47]. Owing to the high specific surface areas, suitable pore sizes and aromatic skeletons, the calix[n]arene-based POPs theoretically exhibit good affinity towards organic dye molecules via intermolecular interactions. For example, Sessler and coworkers [48] prepared three new calix[4]pyrrole-based POPs for removing micropollutants including methylene blue (MB), paraquat and diquat, and the maximum adsorption capacity (q_{max}) for MB is 454 mg g^{-1}; Li and coworkers [49] synthesized a calix[4]arene POP using 1,3,5-tris(4-aminophenyl) benzene as the crosslinker for the efficient adsorption of cationic dyes, and the q_{max} for MB can reach 1806 mg g^{-1}.

Like the above two types of POPs, the currently calixarene-based POPs for removal of organic dyes usually possess high adsorption capacities, but relatively low adsorption rates, no selectivity, even with thermal instabilities, which greatly limit the further development of calixarene-based POPs. Therefore, exploring novel calixarene-based POPs with ultrahigh adsorption capacity, superfast removal rate and excellent selectivity towards organic dyes is of great significance [39].

Herein, we synthesized two novel calix[4]arene-based POPs namely POP-8F and POP-10F through a facile and direct strategy using C-phenylresorcin[4]arene as the building block, and octafluoronaphthalene (abbreviated as M−8F) and decafluorobiphenyl (abbreviated as M−10F) as the crosslinker, respectively. The introduction of the fluorine-rich crosslinkers, M−8F and M−10F is the key novelty in the structures of the calixarene-based POPs, which significantly improves the adsorption performance. Especially M−8F, as far as we know, has not been used as the crosslinker to synthesize calixarene-based POPs in the previously reported literatures. Compared to the commonly used crosslinker, tetrafluoroterephthalonitrile (abbreviated as M−4F) [46], the M−8F has more active sites and more electronegative fluorine atoms, thus the synthesized POP-8F is more negatively charged, which significantly improve the adsorption performance including adsorption rate and maximum adsorption capacity (Table. S1).

Owing to the porous structures, hydrophilicity, good dispersity and abundant active sites, both POP-8F and POP-10F exhibit superfast adsorption rates, ultrahigh adsorption capacities and good selectivity towards cationic dyes. Notably, the adsorption capacity of POP-8F towards Rhodamine B (RhB) can reach 2433 mg g^{-1}. To the best of our knowledge, this is the highest adsorption capacity and surpasses all the previously reported adsorption materials including POPs, COFs, MOFs, porous carbon materials, biomass materials, etc. Benefiting from all the above features, the POP-8F and POP-10F can be promising porous adsorbents and exhibit potential applications in the water treatment and deep purification. Moreover, we also expect the M−8F and M−10F can provide a new avenue for the synthetic strategy of calixarene-based POPs.

2. Experimental section

2.1. Materials

All materials in the synthetic process and the organic pollutants used in the adsorption experiments were purchased from TCI (Shanghai) Development Co. Ltd. All reagents were obtained from Sinopharm Chemical Reagent Co. Ltd and used as received, without further purification, unless otherwise stated.

2.2. Synthetic procedure

2.2.1. Synthesis of monomer

Resorcinol (2.2 g, 20 mmol) and anhydrous ethanol (30 mL) were poured into a 200 mL flask, then concentrated hydrochloric acid (10 mL, 12 M) was added dropwise under stirring and ice-bathing condition. After p-hydroxybenzaldehyde (2.44 g, 20 mmol) was dissolved in 10 mL anhydrous ethanol, the acquired solution was dropwise added into the above reaction system. When finishing dripping, the ice bath was removed and the reaction was heated to reflux for 9 h with stirring. After the reaction was completed, the mixture was cooled to room temperature and filtered, then the filter cake was washed with anhydrous methanol, acetone and ether successfully and dried at 60 ℃ in vacuum to obtain a pink powder with a yield of 72 %. ^{1}H NMR (400 MHz, DMSO-d_6, ppm): δ 7.78 (s, 1H), 7.38 (s, 2H), 5.58 (d, J = 7.6 Hz, 2H), 5.41 (dd, J = 21.1, 13.4 Hz, 3H), 5.02 (s, 1H), 4.46 (s, 1H). (**Fig. S1**) The geometry of the monomer is shown in Scheme S1.

2.2.2. Synthesis of POP-8F and POP-10F

Synthesis of POP-10F: Monomer (0.3 g, 0.35 mmol), potassium carbonate (0.41 g, 3 mmol) and anhydrous DMF (1.5 mL) were added into a 50 mL Schlenk tube. This Schlenk flask was bubbled with nitrogen for 5 min. M−10F (0.334 g, 1 mmol) was dissolved in 10 mL anhydrous THF in another Schlenk flask and also bubbled with nitrogen for at least 5 min, then was added into the above reaction system dropwise with a syringe. Then the tube was degassed by three freeze–pumpthaw cycles, sealed under vacuum and then heated at 85 ℃ for 48 h. After the reaction was completed, the mixture was cooled to room temperature and washed with dilute hydrochloric acid (1 M) until no more bubbles appeared. The obtained mixture was filtered and the filter cake was washed with distilled water, THF and dichloromethane successfully, then the filter cake was dried through freeze-drying with a yield of 62%.

Synthesis of POP-8F: The synthetic procedure of POP-8F was similar to that of POP-10F, only changing the crosslinker to M−8F and the yield was 65%.

The optimal feeding ratio of monomer and crosslinker is 0.35: 1, and the optimal reaction time is 48 h, which are confirmed by q_e and water regain experiments, and the related contents are shown in **Fig. S2-S3** and Table S2.

2.3. Adsorption isotherms

To evaluate the maximum adsorption capacities of (q_{max}) both POP-8F and POP-10F towards different dyes, the adsorption isothermal experiments were taken. In a typical test, 15 mL of the dye solution was charged with 5 mg adsorbents and stirred vigorously until the adsorption equilibrium was reached. Then the UV–Vis spectrophotometry was conducted to calculate the dye concentrations according to the change of the maximum absorbance intensity. The adsorption capacity (q_e, mg g^{-1}) is calculated according to Equation 1:

$$q_e = \frac{C_i\text{-}C_e}{m} V \quad (1)$$

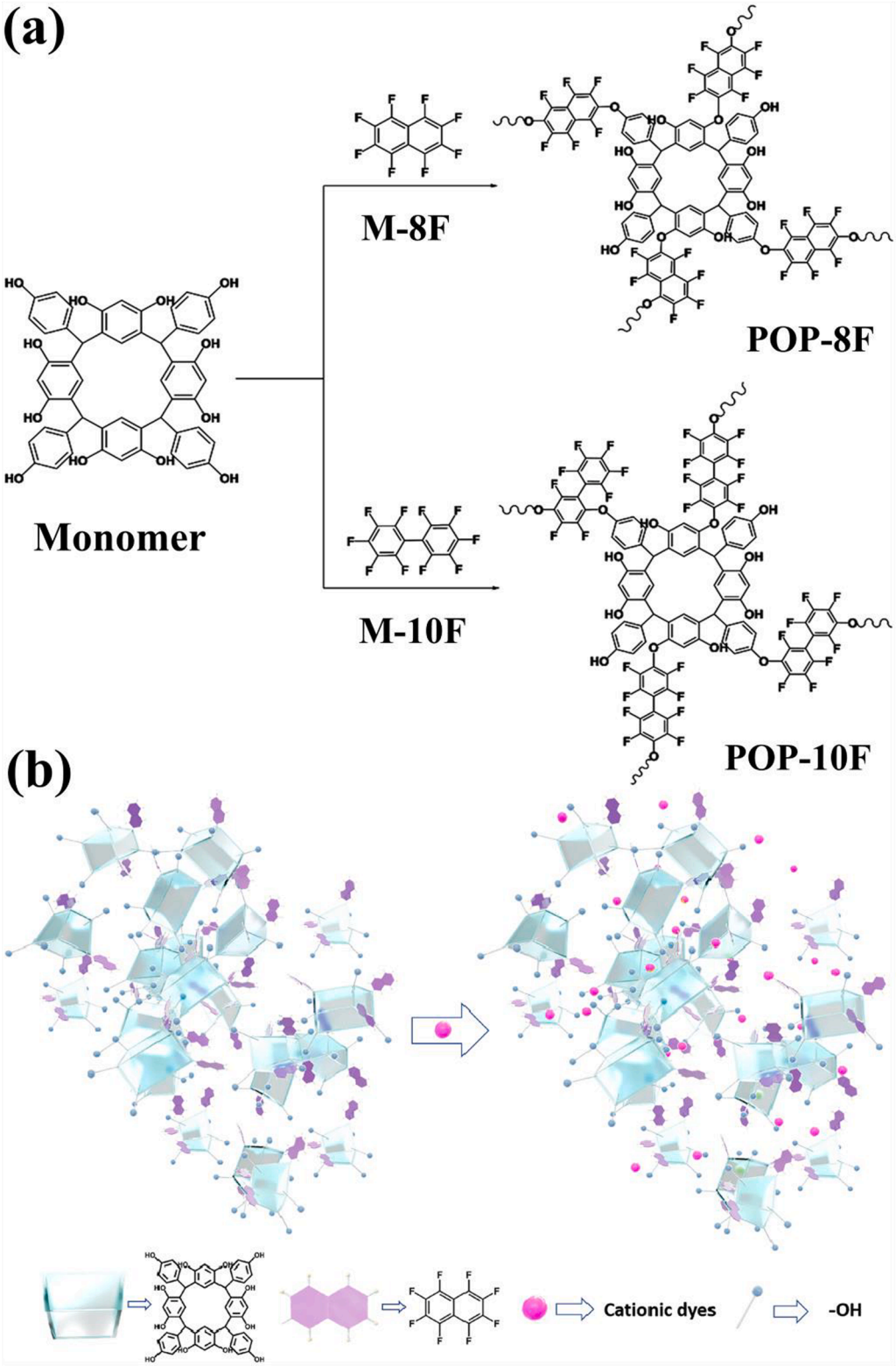

Scheme 1. (a) The design strategy and synthesis route of the calix[4]arene-based polymers, POP-8F and POP-10F. (b) Schematic presentation of the adsorption process of POP-8F towards cationic dyes in aqueous solutions, especially RhB. Sythetic conditions of the POPs: THF, DMF, K_2CO_3, N_2, 85 °C, 48 h.

where C_i and C_e (mg L^{-1}) are the initial and final concentrations of targeted pollutants, m (g) is the weight of the adsorbents used in the adsorption experiments, and V (L) is the volume of the solutions of targeted pollutants.

In this experiment, two adsorption isothermal models including the Freundlich model and the Langmuir model are adopted.

The Freundlich model is:

$$\ln q_e = \ln K_F + \frac{1}{n} \ln C_e \quad (2)$$

The Langmuir model is:

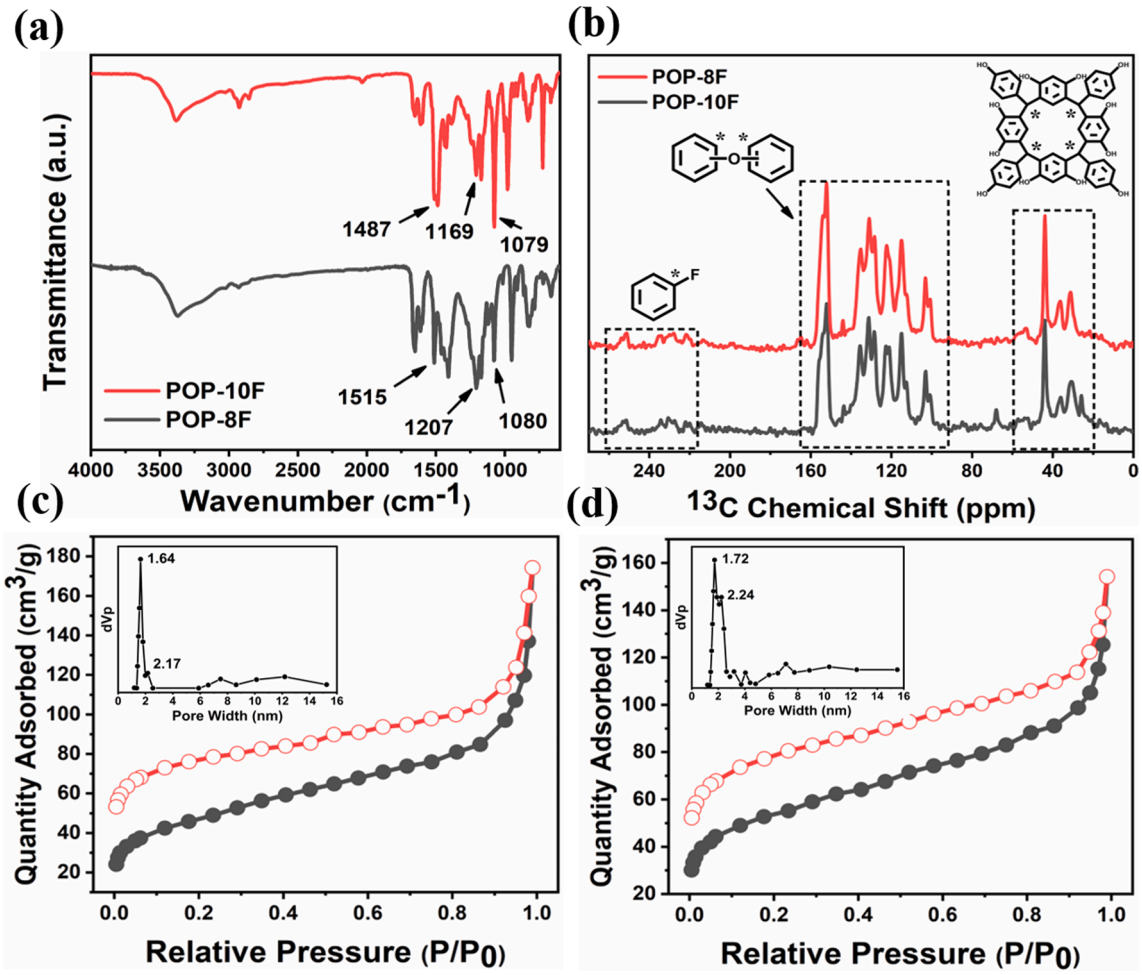

Fig. 1. (a) The FT-IR and (b) solid state ^{13}C NMR spectra of POP-8F and POP-10F; the nitrogen adsorption–desorption isotherm and the corresponding pore size distribution curves of (c) POP-8F and (d) POP-10F.

$$\frac{C_e}{q_e} = \frac{C_e}{q_m} + \frac{1}{K_L q_m} \tag{3}$$

where q_e (mg g^{-1}) is the adsorption capacity in equilibrium; K_F and K_L are the constants of Freundlich and Langmuir models, respectively; 1/n is an empirical parameter of the Freundlich model; C_e (mg g^{-1}) is the concentrations of dyes or phenolic organic pollutants in equilibrium; q_m (mg g^{-1}) is the maximum adsorption capacity under ideal conditions.

2.4. Adsorption kinetics

In a typical experiment, 15 mg POP-8F or POP-10F was added into the dye solutions (50 ppm, 30 mL) and then the mixture was stirred at the rate of 600 rpm at room temperature. At different time intervals, 3 mL of the solution was drawn out and filtered using a 0.22 μm syringe filter to monitor the adsorption process. The UV–Vis spectrophotometer was taken to analyze the UV–Vis spectra of filtrates and the change of maximum absorbance intensity was recorded for further analysis of adsorption kinetics. The adsorption kinetics were analyzed by pseudo-first-order and pseudo-second-order kinetic models.

The pseudo-first-order kinetic model is:

$$\ln(q_e - q_t) = \ln q_e - k_1 t \tag{4}$$

And the pseudo-second-order kinetic model is:

$$\frac{t}{q_t} = \frac{1}{k_2 q_e^2} + \frac{t}{q_e} \tag{5}$$

where q_e (mg g^{-1}) is the adsorption capacity in equilibrium; q_t (mg g^{-1}) is the adsorption capacity in t (min); k_1 (min^{-1}) and k_2 (g mg^{-1} min^{-1}) are the constants of pseudo-first-order and pseudo-second-order models, respectively.

2.5. Dye selective adsorption experiment

To investigate the selective dye adsorption abilities of POP-8F and POP-10F, the cationic dyes including MB, RhB, crystal violet (CV) and the anionic dye methyl orange (MO) were chosen. 20 mL of MB or RhB aqueous solutions (100 ppm) were mixed with 20 mL of MO solution (100 ppm). Then the MB-MO, RhB-MO, RhB-MB and RhB-CV mixtures (all 4 mL) were charged with 4 mg POP-8F or POP-10F and then the resultant mixtures were sonicated for 2 min at room temperature. Afterwards, the mixtures were filtered using 0.22 μm syringe filter and then the changes of UV–Vis spectra were investigated to analyze the selective dye separation properties. All the selective experiments are performed at pH = 3, 7, 11 and the buffer solutions are prepared using 0.1 M HCl or NaOH aqueous solutions.

2.6. Recycling experiment

In a typical recycling experiment, 10 mg POP-8F or POP-10F was added into 10 mL of RhB solution (50 ppm) and stirred for 5 min at the rate of 600 rpm at room temperature. The mixture was centrifuged and the UV–Vis spectrophotometer was taken to calculate the removal efficiency according to Equation 6:

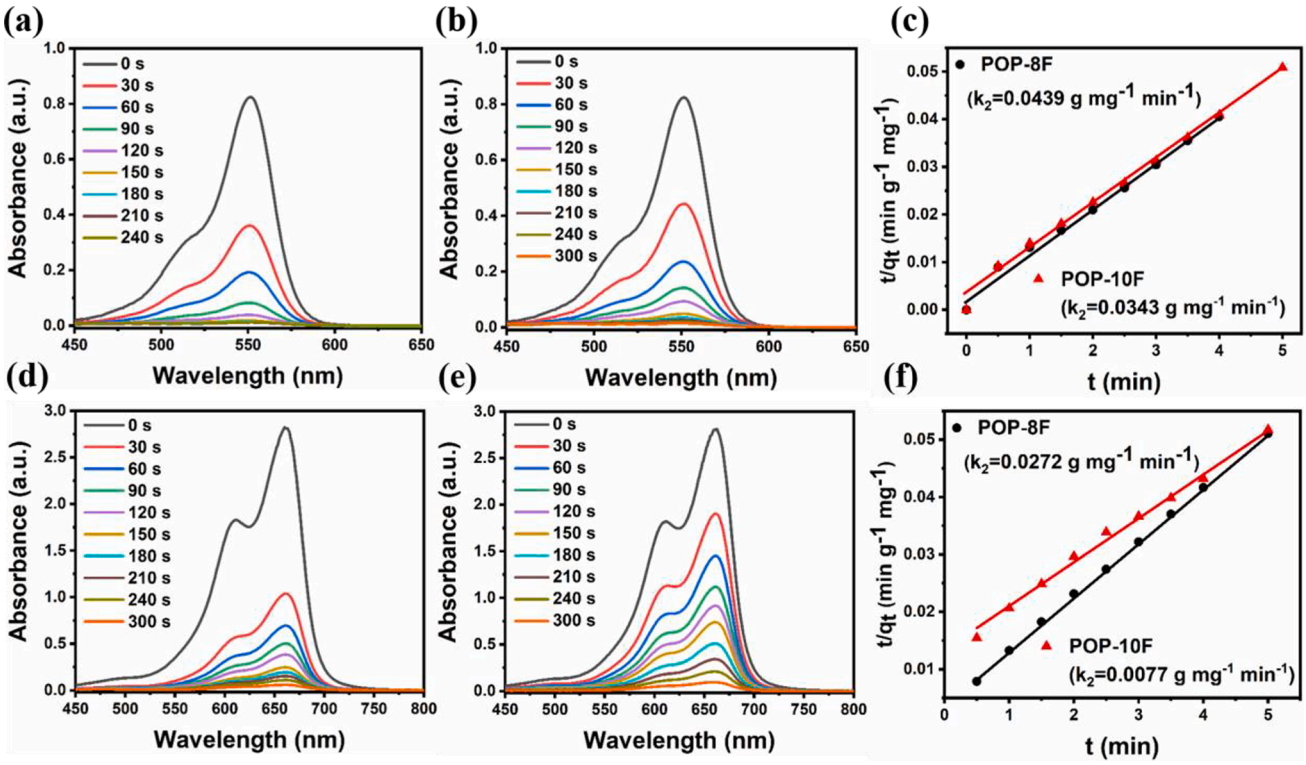

Fig. 2. The changes of UV–Vis spectra of RhB solution (50 ppm) with the addition of (a) POP-8F and (b) POP-10F (both 0.5 mg mL^{-1}) at different time intervals; (c) the pseudo-second-order fitting of adsorption curves of RhB solution with the addition of POP-8F and POP-10F. The changes of UV–Vis spectra of MB solution (50 ppm) with the addition of (d) POP-8F and (e) POP-10F (both 0.5 mg mL^{-1}) at different time intervals; (f) the pseudo-second-order fitting of adsorption curves of MB solution with the addition of POP-8F and POP-10F.

$$\eta = \frac{C_i - C_e}{C_e} \times 100\% \quad (6)$$

where η is the removal efficiency, C_i is the initial concentration of dyes and C_e is the remaining concentration of dyes after the stirring process. Afterwards, the adsorbents were soaked in the ethanol-HCl mixture (1 M HCl) to realize the desorption of RhB from adsorbents. Then the adsorbents were washed with Na_2CO_3 solution (1 M), distilled water and ethanol successfully and dried at 60 ℃ under vacuum for the next cycle.

2.7. Materials characterization

^{1}H NMR spectra were recorded using Bruker-300 NMR spectrometers, with DMSO-d_6 and $CDCl_3$ as the solvent and tetramethylsilane (TMS) as the internal standard at ambient temperature. Solid-state ^{13}C NMR (^{13}C ss-NMR) spectra were recorded on a Bruker INOVA-400 NMR spectrometer at ambient temperature. Power X-ray diffraction (PXRD) of the crosslinking polymers was measured on an X'Pert-Pro MPD to analyze the crystallographic structure of the adsorbent materials. Fourier transform infrared (FT-IR) spectra were tested on a Nicolet-4700 spectrometer. Thermo-gravimetric Analysis (TGA) were carried out on a TA dynamic TGA 2960 instrument, rising from 25 °C to 800 °C with a N_2 flow rate of 50 mL min^{-1} at a heating rate of 10 °C min^{-1}. Scanning electron microscopy (SEM, Hitachi S-4700) together with SEM mapping, and transmission electron microscopy (TEM, Hitachi H600, 200 kV) were employed to observe the morphology, pore sizes, elemental distribution and content of the POPs. The UV–vis spectra were tested using a CARY 50 spectrometer equipped with integrating sphere. The zeta potential was tested on Zetasizer Nano zs laser particle size analyzer at 25 °C and pH = 3, 5, 7, 9, 11.

3. Results and discussion

3.1. Structural characterization

As shown in Scheme 1 and Scheme S2, the calix[4]arene-based porous organic polymers, POP-8F and POP-10F, were synthesized via the reaction between C-phenylresorcin[4]arene and M−8F, M−10F under alkaline and relatively mild conditions. The obtained POPs are hydrophilic and can be well dispersed in water. Moreover, the solubilities of the as-prepared POPs are comparatively poor and insoluble in water and most common organic solvents in our laboratory. Therefore, the structures of both POP-8F and POP-10F are determined via FT-IR and solid state ^{13}C NMR spectra. The results are shown in Fig. 1 **(a-b)**. In the solid state ^{13}C NMR spectra, the crosslinking reactions are random and complicated, thus resulting in the aromatic ether linkages with the multiple peaks at the center of δ = 140 ppm and in the range of δ = 100–160 ppm. The peaks at around δ = 40 ppm and δ = 240 ppm can be ascribed to the alkyl carbons of the monomer and the C-F bonds in the benzene rings, respectively. Moreover, in the FT-IR spectra, the broad peaks in the range of 2900–3000 cm^{-1} and 3000–3600 cm^{-1} are attributed to the stretching vibrations of aromatic C–H bonds and the aromatic hydroxyl groups, respectively. In addition, the peaks at 1487 cm^{-1} and 1515 cm^{-1} are due to the stretching vibrations of the aromatic C = C bonds for POP-10F and POP-8F. For POP-10F, the stretching vibrations of the C-F bonds and C-O-C bonds are located on 1209 cm^{-1} and 1079 cm^{-1}, and those data for POP-8F are 1207 cm^{-1} and 1080 cm^{-1}. Consequently, the results of ^{13}C ss-NMR and FT-IR spectra confirm the successful construction of the polymeric networks.

The thermogravimetric analysis (TGA) spectra of both POP-8F and POP-10F are shown in **Fig. S4**, revealing that the temperatures of POP-8F and POP-10F are 321 ℃ and 247 ℃ when reaching 10 % weight losses. The higher degradation temperature of POP-8F is mainly attributed to the rigidicity of M−8F, that is, the structure of M−8F molecule is

Table 1
The data of adsorption kinetics of POP-8F and POP-10F towards RhB and MB.

Pollutants	Adsorbents	Pseudo-first-order			Pseudo-second-order		
		k_1 (min^{-1})	q_e (mg g^{-1})	R^2	k_2 (g mg^{-1} min^{-1})	q_e (mg g^{-1})	R^2
RhB	POP-8F	1.154	68.450	0.9423	0.04386	105.042	0.9919
	POP-10F	0.8482	68.177	0.9609	0.03425	104.275	0.9933
MB	POP-8F	0.6984	59.638	0.9641	0.02717	105.152	0.9996
	POP-10F	0.6472	106.528	0.9794	0.00771	128.205	0.9939

Table 2
The data of adsorption isotherms of POP-8F and POP-10F towards RhB, MB, CV and MO.

Pollutants	Adsorbents	Langmuir model			Freundlich model		
		K_L (L mg^{-1})	q_m (mg g^{-1})	R^2	1/n	K_F (mg g^{-1})	R^2
RhB	POP-8F	0.1834	2433.08	0.9930	0.1482	1028.70	0.9268
	POP-10F	0.0253	1729.89	0.9905	0.1925	596.16	0.9247
MB	POP-8F	0.0528	862.07	0.9916	0.2702	192.91	0.9803
	POP-10F	0.0317	793.65	0.9897	0.3476	111.63	0.9156
CV	POP-8F	0.0527	1181.02	0.9979	0.0799	691.06	0.9491
	POP-10F	0.0941	925.93	0.9958	0.0738	585.01	0.9085
MO	POP-8F	0.6660	93.721	0.9941	0.0678	70.199	0.9053
	POP-10F	0.4418	89.606	0.9959	0.0902	60.405	0.9179

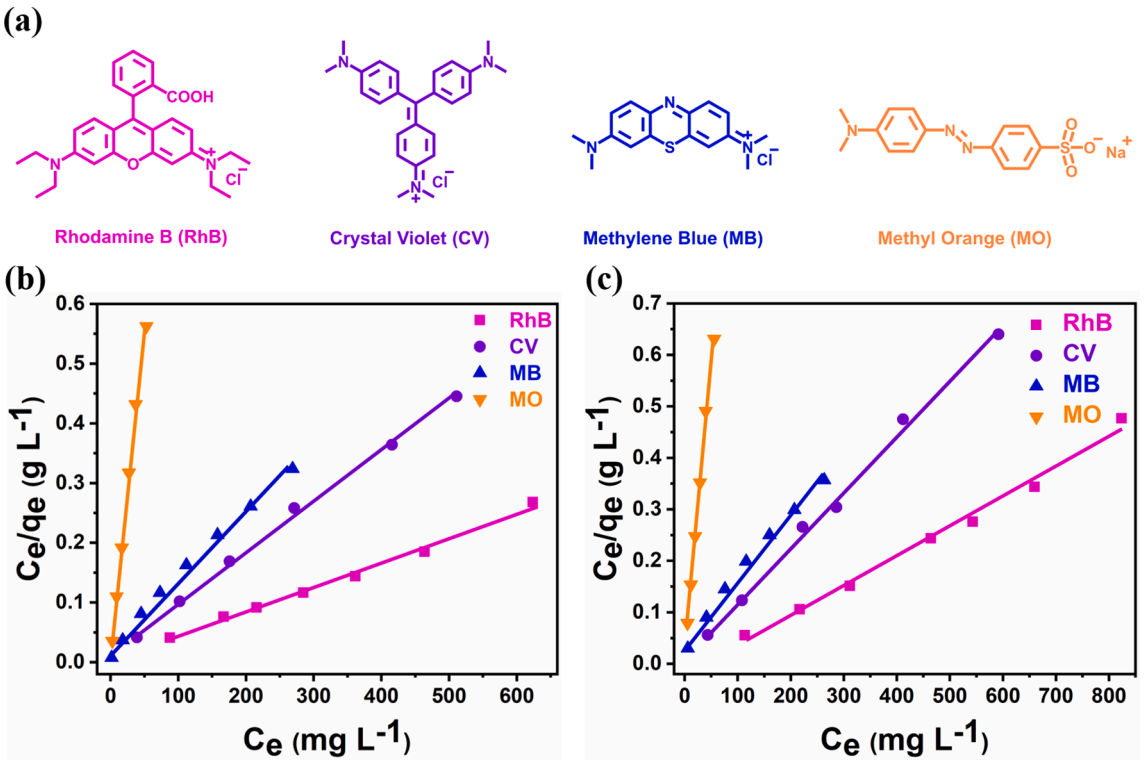

Fig. 3. (a) The chemical structures of organic dyes; the adsorption isotherms of (b) POP-8F and (c) POP-10F towards dyes including RhB, CV, MB and MO.

more rigid than that of M−10F, which further construct more rigid porous skeletons, thus leading to the higher degradation temperature of POP-8F. Moreover, the char yields of POP-8F and POP-10F are 56.8 % and 54.4 % at 600 ℃, respectively, indicating the good thermal stabilities of both POP-8F and POP-10F.

The morphologies of POP-8F and POP-10F are characterized via SEM and TEM. The SEM images show that the morphologies of POP-8F and POP-10F are block-like with rough surfaces, suggesting a porous structure of the polymers. The SEM images also display the irregular porous skeletons of both POP-8F and POP-10F, which can be usually observed in the morphologies of POPs owing to the irregular and unmanageable crosslinking reactions during the preparation process. The TEM images show obvious porous structures with relatively uniform pore sizes (Fig. S5). Additionally, the PXRD curves of both POP-8F and POP-10F show no peaks in the range of small angles, but an obvious and strong peak at about 20° (Fig. S6), indicating that the two POPs both possess amorphous structures and strong intramolecular π-π interactions [49,50].

To further investigate the Brunauer-Emmett-Teller (BET) surface areas (S_{BET}) and pore size distributions of POP-8F and POP-10F, the nitrogen adsorption–desorption experiments were conducted at 77 K and the results are shown in Fig. 1 **(c-d)**. S_{BET} of POP-8F and POP-10F are calculated to be 192.42 and 167.60 m^2 g^{-1}, respectively. Moreover, the micropore and mesopore size distributions of POP-8F are

Table 3
Comparison of some recently reported adsorbents with high maximum adsorption capacities towards RhB.

Adsorbent	q_m (mg g^{-1})	S_{BET} (m^2 g^{-1})	Adsorption mechanism	Reference
DAPS-TP-POP	59.2	4.279	Van der Waals force, hydrogen bonding and electrostatic interactions	[51]
DMPBP[5]	396.1	1347.4	High surface areas	[52]
Biochar meterial	533.77	1156.25	Abundant active groups, high surface area and electrostatic interaction	[53]
aMOC-1	565	unreported	Electrostatic interaction and host–guest interaction	[54]
HPP-1	653.6	1511	High surface areas and π-π interaction	[55]
IL-PVB-pc-80%	693.5	464	Electrostatic interaction and hydrogen bonding	[56]
Chitosan	990	unreported	Abundant amine groups, electrical neutralization effect and bridging adsorption among colloid particles	[57]
POP-O	1012	619	Abundant polar oxygen-containing groups, high surface areas and hierarchical pore structures	[58]
BOPs	1388	unreported	Anion-cation interaction	[59]
AzoPPOP	1357.58	232.72	Electrostatic interaction, existence of $-NH_2$ and π-π interaction	[50]
CTT-POP-1	1160	476	Hydrogen bonding, π-π interaction and electrostatic interaction	[60]
HCPs-5%	1400	1165	High surface areas	[61]
THPP	1402	915	Surface area, hierarchical porous structure and ultra-large pore volume	[62]
HPP-3	1666	1910	Suitable pore size and π-π interaction	[63]
PAF-111	1666	857	High surface areas	[64]
OBPS-HPP-3	1817	1500	High surface areas and π-π interaction	[65]
Py-BF-CMP	1905	1306	Surface area and suitable pore size	[66]
BFTB-PyTA	2127	1133	Surface area, porosity, morphology and π-π interaction	[67]
POP-10F	1729.89	167.60	Electrostatic interaction, suitable pore width, hydrogen bonding andπ-π interaction	This work
POP-8F	2433.08	192.42		

mainly centered at 1.64 nm and 2.17 nm, and the values of POP-10F are 1.72 nm and 2.24 nm. There are also some mesopores located at the range of 4–16 nm. In addition, the total pore volume of POP-8F and POP-10F calculated from the nitrogen gas are 0.202 cm^{-1} g^{-1} and 0.165 cm^{-1} g^{-1}, respectively, indicating both POP-8F and POP-10F possess hierarchical pore structures.

3.2. Adsorption studies of dyes

3.2.1. Adsorption kinetics

Benefiting from the porous structures, high specific surface areas, good thermal stability, highly hydrophilicities (**Fig. S7**) and electronegative natures, as well as the aromatic skeletons and abundant phenolic groups, which can potentially form intermolecualr interaction, such as strong π-π interactions and hydrogen bonding with dyes molecules, both POP-8F and POP-10F are candidates for excellent adsorbents towards cationic dyes.

RhB and MB, as the representative cation dyes, are chosen to investigate the adsorption kinetics of POP-8F and POP-10F. In this experiment, the initial concentration of dyes and adsorbents are 50 ppm and 0.5 mg mL^{-1}. The UV–Vis spectra were recorded to determine the remaining concentrations at different time intervals upon the addition of adsorbents. As shown in Fig. 2 and **Fig. S8**, for RhB, the removal efficiencies are 76.76 % (POP-8F) and 71.40 % (POP-10F) when stirring for 1 min, and the data can reach 98.57 % for POP-8F within 4 min and 98.26 % for POP-10F within 5 min, both nearly completely adsorption. Moreover, for MB, the removal efficiencies are 75.43 % (POP-8F) and 48.44 % (POP-10F) when stirring for 1 min, and the data can reach 97.89 % for POP-8F and 96.66 % for POP-10F when time is 5 min. To investigate the adsorption kinetics of both POP-8F and POP-10F, pseudo-first-order and pseudo-second-order kinetic models are adopted and the detailed data are summarized in Table 1. The correlation coefficient values (R^2) of pseudo-second-order for POP-8F towards RhB and MB are 0.9919 and 0.9996, and those for POP-10F towards RhB and MB are 0.9933 and 0.9939, respectively. The R^2 of pseudo-second-order model for both POP-8F and POP-10F are close to 1 and higher than the values of their corresponding pseudo-first-order model, indicating the time-dependent adsorption process of RhB fits better with pseudo-second-order model and chemical adsorption is the main factor influencing the adsorption rate. In addition, the pseudo-second-order constant (k_2) of POP-8F for RhB is 0.044 g mg^{-1} min^{-1}, which is higher than that of POP-10F (0.034 g mg^{-1} min^{-1}); the k_2 of POP-8F for MB is 0.027 g mg^{-1} min^{-1}, which is nearly four times higher than that of POP-10F (0.007 g mg^{-1} min^{-1}). Moreover, the comparison of k_2 of POP-8F and POP-10F with other reported adsorption materials is shown in Table S3. The results shows the k_2 of POP-8F is higher than that of POP-10F, indicating the faster adsorption rate of POP-8F, and considering the k_2 of POP-8F is higher than majority of other reported adsorbents, demonstrating the POP-8F is a more promising adsorption material for the ultrafast removal of cationic dyes from wastewater.

3.2.2. Adsorption isotherms

The adsorption isotherms and capacities are usually used to determine the adsorption mechanisms and abilities of the adsorption materials. In this experiment, the maximum adsorption capacities (q_{max}) of both POP-8F and POP-10F towards three cationic dyes MB, RhB, CV and one anionic dye MO have been investigated. 5 mg of adsorbents were added into 15 mL of dyes solutions with different initial concentrations (RhB: 800–1400 ppm; CV: 300–800 ppm; MB: 100–550 ppm; MO: 30–80 ppm) and then vigorously stirred until the adsorption equilibrium reached. Afterwards, the data of equilibrium concentration (C_e) and adsorption capacity (q_e) were fitted by the Langmuir and Freundlich models. The isotherm parameters are summarized in Table 2 and more details are displayed in Fig. 3, **Fig. S9-S13**.

As listed in Table 2, the correlation coefficients (R^2) of Langmuir models (POP-8F: 0.9930 for RhB, 0.9916 for MB, 0.9979 for CV; POP-10F: 0.9905 for RhB, 0.9897 for MB, 0.9958 for CV) are approximately 1 and higher than their corresponding R^2 of Freundlich models (POP-8F: 0.9268 for RhB, 0.9803 for MB, 0.9491 for CV; POP-10F: 0.9247 for RhB, 0.9156 for MB, 0.9085 for CV), indicating the Langmuir isotherm model can more accurately describe the adsorption performance of both POP-8F and PO-10F. Meanwhile, it means the adsorption process of the organic dyes is primarily monolayer and homogeneous adsorption. Moreover, both POP-8F and POP-10F exhibit more affinity and much higher adsorption capacities towards cationic dyes than anionic dyes. The q_{max} of POP-10F calculated from the Langmuir equation reaches 793.65, 1729.89, 925.93 mg g^{-1} for MB, RhB, CV respectively. The q_{max} of POP-8F is higher and reaches 862.07, 2433.08, 1181.02 mg g^{-1} for MB, RhB, CV respectively. Clearly, both POP-8F and POP-10F exhibit the highest adsorption capacities towards RhB, thus the q_{max} of both POP-8F and POP-10F are comparable with some other excellent recently published adsorbents and the results are shown in Table 3. Notably, as far as we know, the maximum adsorption capacity of POP-8F (2433.08 mg g^{-1}) is higher than the values of all the previously reported adsorption materials, including POPs, COFs, MOFs,

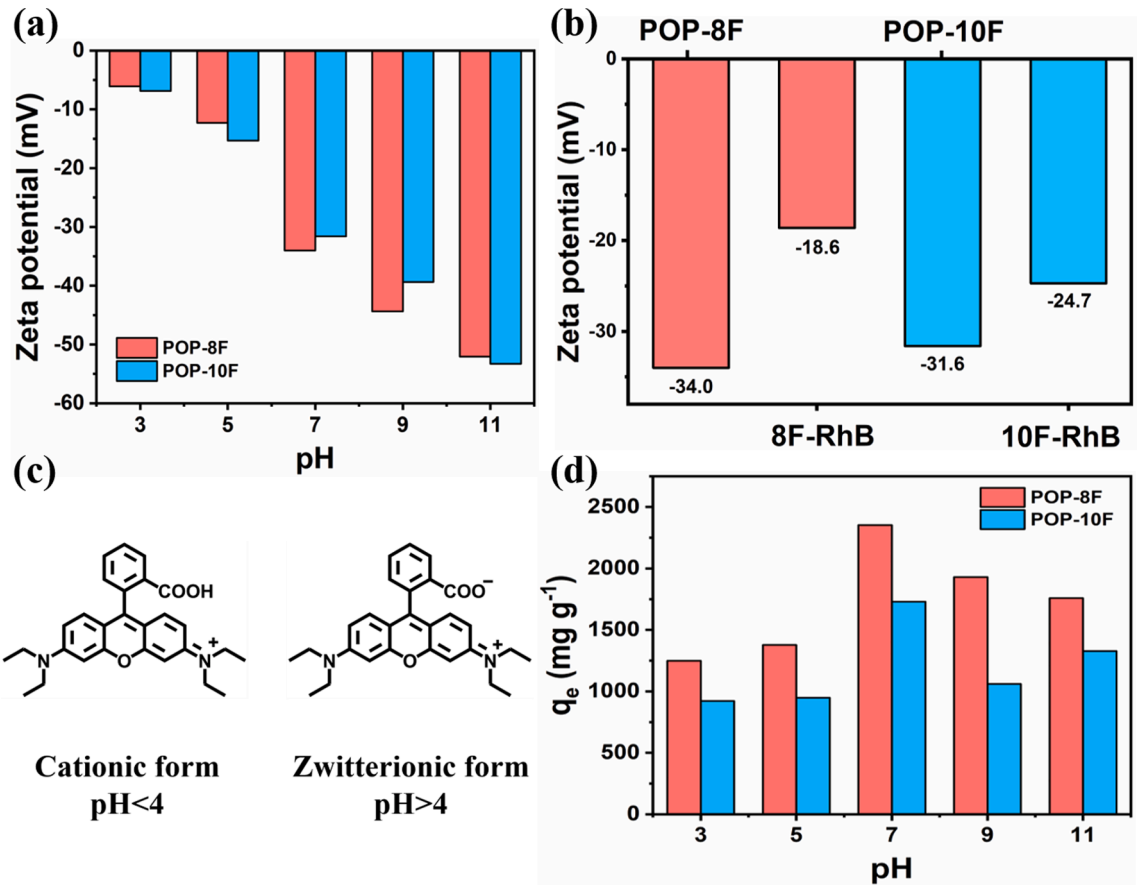

Fig. 4. (a) The zeta potentials of POP-8F and POP-10F at different pH at 25 °C; (b) The zeta potentials of POP-8F and POP-10F before and after the adsorption of RhB at 25 °C and pH = 7; (c) The different forms of RhB under different pH conditions; (d) The q_e of POP-8F and POP-10F at different pH.

biomass adsorbents, activated carbon materials, etc, demonstrating the superiority of POP-8F and its potential application in ultrafast and highly-efficient removal of cationic dyes from water.

3.2.3. *Adsorption mechanisms*

Under neutral conditions, the zeta potentials of POP-8F and POP-10F are −34.0 mV and −31.6 mV, respectively, indicating that the POPs are negatively charged with electronegative natures (Fig. 4**a**). Under acidic and alkaline conditions (pH = 3, 5, 9, 11), both POP-8F and POP-10F are also negatively charged, more easily combining with cationic dyes via an electrostatic interaction, thus explaining the lowest adsorption capacities towards anionic dye MO. As shown in Fig. 4 **(b)**, the zeta potentials of the POPs after adsorption of RhB increase a lot compared with the values before adsorption, further indicating the electrostatic interaction plays an important role in the adsorption mechanism. Moreover, the electrostatic interaction can also be proved by the changes in the FT-IR spectra before and after the adsorption process (**Fig. S14**). The peaks at 1207 cm^{-1} for POP-8F and 1209 cm^{-1} for POP-10F are attributed to the aromatic C-F bonds, and these peaks substantially decrease after the adsorption of cationic dyes, demonstrating the formation of fluorine-cation interaction resulting from the abundant electronegative fluorine atoms in POP-8F and POP-10F [46].

However, as shown in Fig. 4 **(c, d)**, when pH > 4, RhB has a zwitterionic form, which goes against the adsorption performance owing to the charge repulsion. With the further increasing pH (pH > 7), RhB is inclined to aggregate and form a dimer structure with a larger molecular size, increasing the difficulty of entering into the porous skeletons of the POPs [68]. However, the q_e of POP-8F and POP-10F still reach 1758 and 1327 mg g^{-1} at pH = 11, respectively, demonstrating the electrostatic interaction is not the only reason for the excellent adsorption performances of the POPs.

The peak position shifts corresponding to the aromatic C = C bonds in the FT-IR spectra are also obvious. As the green lines show, the peaks attributed to the aromatic C = C bonds at 1510, 1614 cm^{-1} for POP-8F and 1510, 1612 cm^{-1} for POP-10F slightly shift after adsorption of RhB, MB and CV, proving the π-π stacking interaction and/or electrostatic interactions between the POPs and cationic dyes [67]. The peaks at 36 ppm for POP-8F and 36 ppm, 31 ppm for POP-10F obviously decrease or completely disappear after adsorption of cationic dyes in the solid state ^{13}C NMR spectra, while the peaks located at other places remain the same (**Fig. S15**). These changed peaks are attributed to the alkyl carbons of the calixarene-based skeletons, and the decrease or disappearance of these peaks indicate that some of the cationic dyes are probably adsorbed and trapped in the pores of calixarene-based skeletons, thus leading to the changes of chemical environment of the alkyl carbons, and demonstrating the importance of the porous structures and the successful adsorption of cationic dyes.

Moreover, the different adsorption capacities of POP-8F and POP-10F towards cationic dyes are also related to the different molecular sizes of RhB, MB, CV, and the detailed information is shown in Table S4. The adsorption capacities follow the order of RhB > CV > MB, in accordance with the order of cationic dye molecular sizes RhB (1.59 × 1.18 × 0.56 nm^3) > CV (1.41 × 1.21 × 0.18 nm^3) > MB (1.26 × 0.77 × 0.65 nm^3) [60]. The BET analysis exhibits that the pore size distributions of POP-8F and POP-10F are centered at 1.64 and 1.72 nm. For MB, a cationic dye with smaller size, it is too small to be captured and can easily leave the pores, thus the adsorption capacity of MB is the lowest among the three characteristic cationic dyes. While the RhB molecules with relatively larger size can block the micropores and bind in the mesopores, thus resulting in the higher adsorption capacities. In

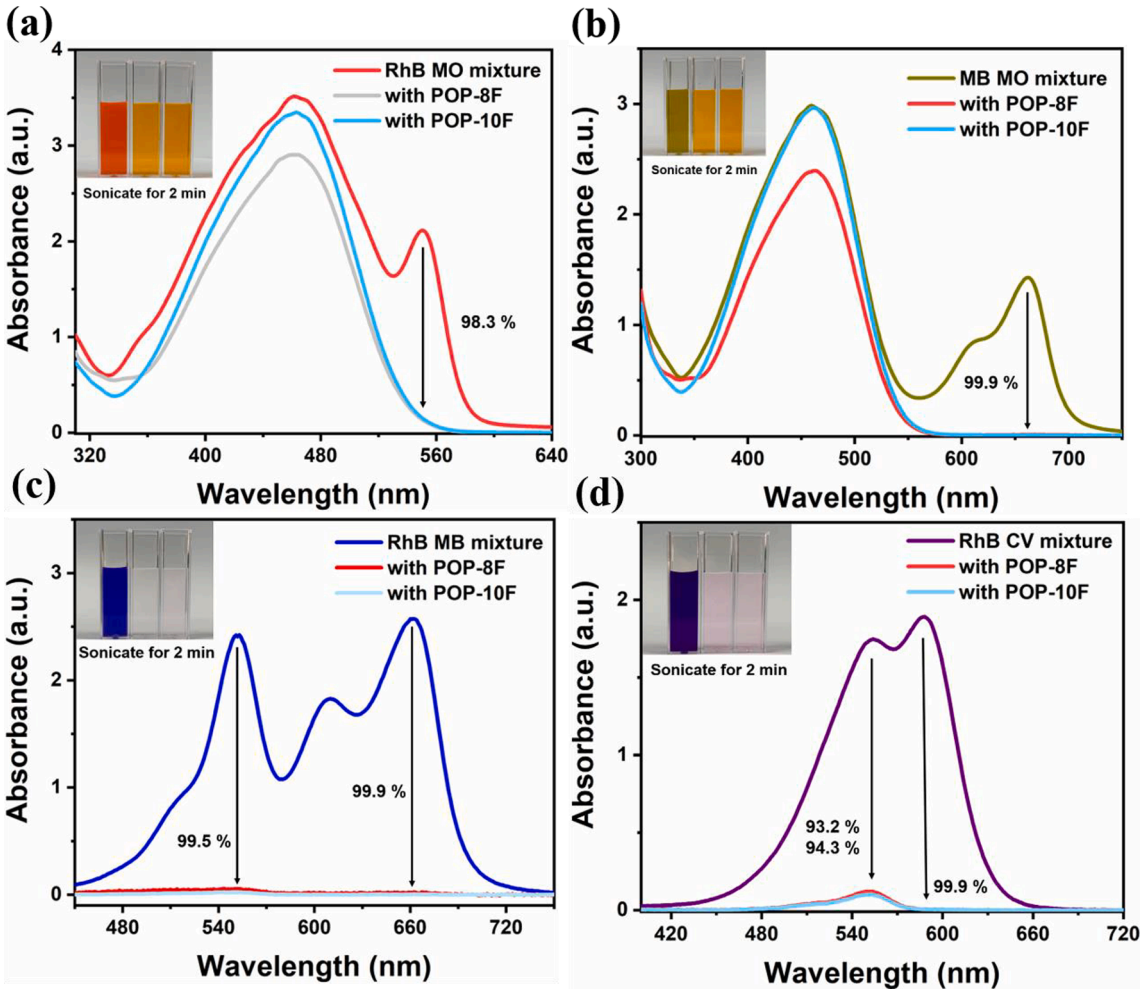

Fig. 5. Change of the UV–Vis spectra of (a) RhB-MO, (b) MB-MO, (c) RhB-MB and (d) RhB-CV mixtures at pH = 7 with the addition of POP-8F or POP-10F. Inset: for each image, left: the original mixture; middle: after adsorption using POP-8F; right: after adsorption using POP-10F.

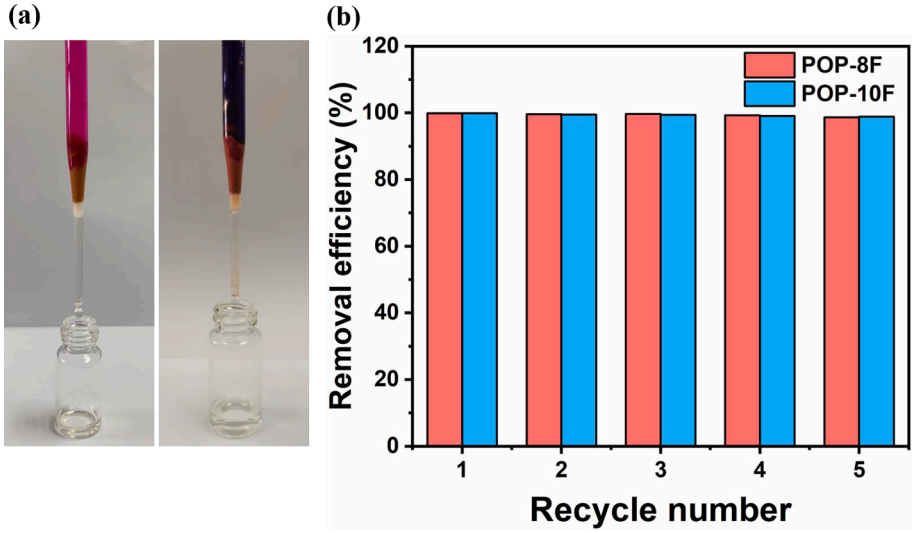

Fig. 6. (a) Images of simulated column adsorption devices. Left: RhB solution, 500 ppm; Right: a mixture of RhB, MB, CV, all 500 ppm. (b)The removal efficiencies of POP-8F and POP-10F towards RhB (50 ppm) after five cycles.

addition, the hydrogen bonding formed between the carboxyl group of RhB and the residual phenolic hydroxyl groups of POPs also contributes to the higher adsorption capacities towards RhB.

Consequently, the electrostatic interaction, porous structures and π-π stacking interaction contribute to the excellent adsorption performance of POP-8F and POP-10F towards cationic dyes, and the hydrogen

bonding and suitable molecular size further result in the highest adsorption capacities towards RhB.

Additionally, compared with POP-10F, POP-8F possess higher surface area, smaller pore sizes, lower zeta potentials, endowing POP-8F more spaces and more electronegative natures for adsorption. Furthermore, the pore width of POP-8F is more suitable for the adsorption of cationic dyes. Therefore, these factors all contribute to the better adsorption performance of POP-8F.

3.2.4. Dye selective adsorption

An excellent adsorbent should not only possess the disadvantage of high adsorption capacity, high removal efficiency, fast adsorption rate, hypotoxicity, but also good dye selective adsorption properties. According to the results in Section 3.2.2, both POP-8F and POP-10F display extremely high adsorption capacities towards cationic dyes including RhB, MB and CV, but much lower adsorption capacities towards anionic dyes such as MO. Therefore, POP-8F and POP-10F might be promising adsorbents for separating charged dyes. Moreover, the selectivity between different cation dyes were also investigated. All the selective experiments were performed at pH = 3, 7, 11 to investigate the selective performance of the POPs under different pH, and the images of each individual target dye at different pH are shown in **Fig. S16**.

When at pH = 7, the selectivity between dyes with opposite charges are remarkable and the performances are displayed in Fig. 5. For RhB-MO mixture, after being sonicated for 2 min, the η of POP-8F and POP-10F towards RhB reach 98.3 %, while those for MO are only 17.4 % and 4.9 %, respectively. For MB-MO mixture, the η of both adsorbents can reach 99.9 %, approaching complete adsorption, but those for MO are 20.0 % and 0.96 %, respectively, demonstrating the extraordinary selectivity between the cationic dyes and anionic dyes. Additionally, for mixtures containing different cationic dyes, the adsorption rates of adsorbents towards MB and CV are faster than those towards RhB. For RhB-MB mixtures, after being sonicated for 2 min, the η of both POP-8F and POP-10F towards MB reach 99.9 %, but those towards RhB are 99.5 % with a very light pink residual color. And for RhB-CV mixtures, although the η towards CV are 99.9 %, but those towards RhB are only 93.2 % and 94.3 %, respectively, and the residual pink color of RhB is obvious. The faster adsorption rates towards MB and CV can be mainly attributed to the smaller molecular sizes (details listed in Table. S2), compared with RhB, which allows MB and CV molecules more easily diffuse into the porous skeletons of the adsorbents. In addition, the selective adsorption performance of POP-8F and POP-10F at pH = 3, 11 are almost the same and the detailed graphs are displayed in **Fig. S17-S18**, indicating the excellent charge selective abilities of POP-8F and POP-10F under acidic, neutral and alkaline conditions.

3.3. Purification of simulated industrial wastewater

The real industrial wastewater usually contains several types of pollutants, hence the removal rate, removal efficiency and selective adsorption capability of multi-component pollutants are significant factors for evaluating the adsorption performance of adsorbents. Therefore, a column adsorption experiment was chosen as a simulator to investigate the potential application in purification of real wastewater and POP-8F was chosen for this experiment. As shown in Fig. 6 **(a)**, 20 mL of RhB solution (500 ppm) was passed through a column filled with 50 mg POP-8F without air pressure, the solution turns to colorless immediately, which can be clearly observed with naked eyes. In addition, a mixture of cationic dyes including RhB, MB and CV (500 ppm) can also be completely adsorbed through the column and the purple color absolutely disappears. These results demonstrate the calixarene-based POPs have the practical applications in the sewage treatment.

3.4. Recycling experiments and cost analysis

Finally, we investigate the recyclability and reusability of POP-8F and POP-10F, which are crucial indicators for the potential practical applications of adsorbents. Considering POP-8F and POP-10F showing highest adsorption capacities and adsorption rates towards RhB, it is chosen as a representative pollutant to investigate the desorption and recyclability properties of the adsorbents. 10 mL of RhB solution (50 ppm) was stirred for 5 min with the addition of 10 mg adsorbents to prove the adsorption equilibrium had been reached. After adsorption, the RhB can be easily released by soaking the adsorbents into ethanol containing 1 M HCl and continuously washed with 1 M sodium carbonate solution, distilled water and ethanol. As shown in Fig. 6 **(b),** after five cycles, both POP-8F and POP-10F maintain excellent removal efficiencies, only slightly decrease from 99.9 % to 98.7 % and 98.9 %, respectively. The minor weight loss of adsorbents during the recycling process is inevitable, and the RhB molecules might not be completely desorbed, thus these two factors mainly contribute to the slight decline of removal efficiencies. In addition, the FT-IR spectra of both POP-8F and POP-10F after five cycles are shown in **Fig. S19**. The spectra after five cycles match well with those of the original adsorbents, confirming the good stabilities of both POP-8F and POP-10F. Consequently, owing to the high removal efficiency and easy regeneration, POP-8F and POP-10F might be excellent candidates for the adsorbents used in water treatment and purification.

Additionally, if industrial applications are required, the cost analysis of these two novel adsorbents is of great concern. As shown in Table S5-S7, we have taken all the raw materials and solvents into account, and the cost of POP-8F and POP-10F are estimated to be 46 $ kg^{-1} and 49 $ kg^{-1}, respectively, which are higher than standard and advanced commertial Activated carbons (ACs), but are almost the same with some ACs with high qualities. However, considering higher q_m, higher adsorption rates, excellent selectivities and convenient reusabilities of POP-8F and POP-10F, the two novel adsorbents are expected to be ecnomically competative with ACs when wholescale production is performed.

4. Conclusion

In summary, two novel calixarene-based porous organic polymers namely POP-8F and POP-10F using C-phenylresorcin[4]arene and two types of perfluoro-aromatic compounds as the monomers were successfully synthesized via a simple and mild crosslinking reaction. The introduction of crosslinker M−8F and M−10F is the key novelty of this work. The obtained POPs have the advantages of the porous structures, abundant active sites, good thermal stability and electronegative natures. These advantages endow both POP-8F and POP-10F with extraordinary adsorption properties including ultrafast adsorption rates, extremely high adsorption capacity, good reusability and remarkable selectivity towards cationic dyes. The pseudo-second-order rate constant of POP-8F towards RhB is 0.04386 g mg^{-1} min^{-1}, higher than most recently reported POPs. Notably, the maximum adsorption capacity of POP-8F towards RhB can be up to 2433 mg g^{-1}, outpacing all the previously reported porous adsorbents including COFs, MOFs, POPs, bio-adsorbents, activated carbons, etc. Owing to the above prominent characteristics, the novel calixarene-based POP-8F and POP-10F can be promising adsorbents and potentially used in the application of water pollutant treatment and wastewater efficient purification.

Declaration of Competing Interest

The authors declare that they have no known competing financial interests or personal relationships that could have appeared to influence the work reported in this paper.

Acknowledgements

We sincerely acknowledge financial support from the National Natural Science Foundation of China (21938006, 51773144), Science Foundation of Jiangsu Province (BE2019659), Basic Research Project of

Leading Technology (BK20202012) and PAPD in Jiangsu Province.

Appendix A. Supplementary data

Supplementary data to this article can be found online at https://doi.org/10.1016/j.cej.2021.134442.

References

[1] B. Petrie, R. Barden, B. Kasprzyk-Hordern, A review on emerging contaminants in wastewaters and the environment: current knowledge, understudied areas and recommendations for future monitoring, Water Res. 72 (2015) 3–27.

[2] S.Y. Kimura, S.D. Richardson, Water analysis: emerging contaminants and current issues, Anal. chem 88 (2016) 546–582.

[3] J. Yeston, R. Coontz, J. Smith, C. Ash, A thirsty world, Science 313 (2006) 1067.

[4] Y. Luo, W. Guo, H.H. Ngo, L.D. Nghiem, F.I. Hai, J. Zhang, S. Liang, X.C. Wang, A review on the occurrence of micropollutants in the aquatic environment and their fate and removal during wastewater treatment, Sci. Total Environ. 473-474 (2014) 619–641.

[5] K.E. Murray, S.M. Thomas, A.A. Bodour, Prioritizing research for trace pollutants and emerging contaminants in the freshwater environment, Environ. Pollut. 158 (12) (2010) 3462–3471.

[6] R. Bera, M. Ansari, S. Mondal, N. Das, Selective CO_2 capture and versatile dye adsorption using a microporous polymer with triptycene and 1,2,3-triazole motifs, Eur. Polym. J. 99 (2018) 259–267.

[7] C. Zhang, P.-C. Zhu, L. Tan, J.-M. Liu, B. Tan, X.-L. Yang, H.-B. Xu, Triptycene-Based Hyper-Cross-Linked Polymer Sponge for Gas Storage and Water Treatment, Macromolecules 48 (23) (2015) 8509–8514.

[8] Y. Liu, Y. Cui, C. Zhang, J. Du, S. Wang, Y. Bai, Z. Liang, X. Song, Post-cationic Modification of a Pyrimidine-Based Conjugated Microporous Polymer for Enhancing the Removal Performance of Anionic Dyes in Water, Eur. Polym. J. 24 (29) (2018) 7480–7488.

[9] R. Shen, X. Yan, Y.-J. Guan, W. Zhu, T. Li, X.-G. Liu, Y. Li, Z.-G. Gu, One-pot synthesis of a highly porous anionic hypercrosslinked polymer for ultrafast adsorption of organic pollutants, Polym. Chem 9 (38) (2018) 4724–4732.

[10] J. Liu, S. Zhou, P. Gu, T. Zhang, D. Chen, N. Li, Q. Xu, J. Lu, Conjugate Polymer-clothed TiO_2@V_2O_5 nanobelts and their enhanced visible light photocatalytic performance in water remediation, J. Colloid Interface Sci. 578 (2020) 402–411.

[11] L. Qian, F.D. Kopinke, T. Scherzer, J. Griebel, A. Georgi, Enhanced degradation of perfluorooctanoic acid by heat-activated persulfate in the presence of zeolites, Chem. Eng. J. 429 (2022), 132500.

[12] R. Ji, J. Liu, T. Zhang, Y. Peng, Y. Li, D. Chen, Q. Xu, J. Lu, Construction of a ternary Z-scheme In_2S_3@Au@P3HT photocatalyst for the degradation of phenolic pollutants under visible light, Sep. Purif. Technol. 272 (2021), 118787.

[13] D.P. Zagklis, A.I. Vavouraki, M.E. Kornaros, C.A. Paraskeva, Purification of olive mill wastewater phenols through membrane filtration and resin adsorption/desorption, J. Hazard. Mater. 285 (2015) 69–76.

[14] L.i. Zhao, Y. Ji, D. Kong, J. Lu, Q. Zhou, X. Yin, Simultaneous removal of bisphenol A and phosphate in zero-valent iron activated persulfate oxidation process, Chem. Eng. J. 303 (2016) 458–466.

[15] Y. Zhu, P. Gu, H. Wan, S. Zhou, J. He, H. Li, N. Li, Q. Xu, J. Lu, SuFEx modification of silk fibroin silicon aerogel and its adsorption behavior and antibacterial performance, Chemosphere 287 (2022), 132291.

[16] A. Cruz Del Alamo, M.I. Pariente, F. Martinez, R. Molina, Trametes versicolor immobilized on rotating biological contactors as alternative biological treatment for the removal of emerging concern micropollutants, Water Res. 170 (2020), 115313.

[17] Q. Huang, K. Chai, L. Zhou, H. Ji, A phenyl-rich β-cyclodextrin porous crosslinked polymer for efficient removal of aromatic pollutants: Insight into adsorption performance and mechanism, Chem. Eng. J. 387 (2020), 124020.

[18] L. Chen, M. Rong, L. Yang, J. Yu, H. Qu, Q. Meng, S. Ni, Z. Xu, X. Zhu, L. Wang, H. Xing, H. Liu, Construction of super-hydrophobic hypercrosslinked porous polymers for selectively removing aromatic diamines from the polyurethane bio-hydrolysate, Chem. Eng. J. 428 (2022), 132509.

[19] A. Alsbaiee, B.J. Smith, L. Xiao, Y. Ling, D.E. Helbling, W.R. Dichtel, Rapid removal of organic micropollutants from water by a porous beta-cyclodextrin polymer, Nature 529 (7585) (2016) 190–194.

[20] W. Ji, Y.S. Guo, H.M. Xie, X. Wang, X. Jiang, D.S. Guo, Rapid microwave synthesis of dioxin-linked covalent organic framework for efficient micro-extraction of perfluorinated alkyl substances from water, J. Hazard. Mater. 397 (2020), 122793.

[21] Y. Li, Z. Yang, Y. Wang, Z. Bai, T. Zheng, X. Dai, S. Liu, D. Gui, W. Liu, M. Chen, L. Chen, J. Diwu, L. Zhu, R. Zhou, Z. Chai, T.E. Albrecht-Schmitt, S. Wang, A mesoporous cationic thorium-organic framework that rapidly traps anionic persistent organic pollutants, Nat Commun 8 (1) (2017) 1354.

[22] S.T.M.L.D. Senevirathna, S. Tanaka, S. Fujii, C. Kunacheva, H. Harada, B. R. Shivakoti, R. Okamoto, A comparative study of adsorption of perfluorooctane sulfonate (PFOS) onto granular activated carbon, ion-exchange polymers and non-ion-exchange polymers, Chemosphere 80 (6) (2010) 647–651.

[23] B. Wang, X. Yang, L. Ma, L. Zhai, J. Xuan, C. Liu, Z. Bai, Ultra-high efficient pH induced selective removal of cationic and anionic dyes from complex coexisted solution by novel amphoteric biocomposite microspheres, Sep. Purif. Technol. 231 (2020), 115922.

[24] H.-R. Kim, J.-W. Jang, J.-W. Park, Carboxymethyl chitosan-modified magnetic-cored dendrimer as an amphoteric adsorbent, J. Hazard. Mater. 317 (2016) 608–616.

[25] Y. Tu, G. Xu, L. Jiang, X. Hu, J. Xu, X. Xie, A. Li, Amphiphilic hyper-crosslinked porous cyclodextrin polymer with high specific surface area for rapid removal of organic micropollutants, Chem. Eng. J. 382 (2020), 123015.

[26] H. Shan, S. Li, Z. Yang, X. Zhang, Y. Zhuang, Q. Zhu, D. Cai, P. Qin, J. Baeyens, Triazine-based N-rich porous covalent organic polymer for the effective detection and removal of Hg (II) from an aqueous solution, Chem. Eng. J. 426 (2021), 130757.

[27] X. Zheng, Q. Ruan, Q. Jiang, K. Wang, Q. Wang, Y. Tang, H. Huang, C. Zhong, Integrated adsorption and catalytic degradation of safranine T by a porous covalent triazine-based framework, J. Colloid Interface Sci. 532 (2018) 1–11.

[28] S. Che, L. Fang, Porous Ladder Polymer Networks, Chem 6 (10) (2020) 2558–2590.

[29] W. Ji, T.-X. Wang, X. Ding, S. Lei, B.-H. Han, Porphyrin- and phthalocyanine-based porous organic polymers: From synthesis to application, Coord. Chem. Rev. 439 (2021) 213875, https://doi.org/10.1016/j.ccr.2021.213875.

[30] J. Jia, Z. Chen, H. Jiang, Y. Belmabkhout, G. Mouchaham, H. Aggarwal, K. Adil, E. Abou-Hamad, J. Czaban-Jóźwiak, M.R. Tchalala, M. Eddaoudi, Extremely Hydrophobic POPs to Access Highly Porous Storage Media and Capturing Agent for Organic Vapors, Chem 5 (1) (2019) 180–191.

[31] S. Wang, X. Hai, X. Ding, S. Jin, Y. Xiang, P. Wang, B. Jiang, F. Ichihara, M. Oshikiri, X. Meng, Y. Li, W. Matsuda, J. Ma, S. Seki, X. Wang, H. Huang, Y. Wada, H. Chen, J. Ye, Intermolecular cascaded π-conjugation channels for electron delivery powering CO_2 photoreduction, Nat Commun 11 (1) (2020) 1149.

[32] J. Liu, K.-K. Yee, K.-W. Lo, K.Y. Zhang, W.-P. To, C.-M. Che, Z. Xu, Selective Ag(I) binding, H2S sensing, and white-light emission from an easy-to-make porous conjugated polymer, J. Am. Chem. Soc. 136 (7) (2014) 2818–2824.

[33] J. Wu, F. Xu, S. Li, P. Ma, X. Zhang, Q. Liu, R. Fu, D. Wu, Porous Polymers as Multifunctional Material Platforms toward Task-Specific Applications, Adv. Mater. 31 (4) (2019) 1802922, https://doi.org/10.1002/adma.v31.410.1002/adma.201802922.

[34] S. Zhou, P. Gu, H. Wan, Y. Zhu, N. Li, D. Chen, A. Marcomini, Q. Xu, J. Lu, Preparation of new triptycene- and pentiptycene-based crosslinked polymers and their adsorption behavior towards aqueous dyes and phenolic organic pollutants, Sep. Purif. Technol. 278 (2022), 119495.

[35] H. Deng, B. Zhang, Y. Xu, Y. Zhang, J. Huo, L. Zhang, G. Chang, A simple approach to prepare isoxazoline-based porous polymer for the highly effective adsorption of 2,4,6-trinitrotoluene (TNT): Catalyst-free click polymerization between an in situ generated nitrile oxide with polybutadiene, Chem. Eng. J. 393 (2020), 124674.

[36] X. Suo, Y. Yu, S. Qian, L. Zhou, X. Cui, H. Xing, Tailoring the Pore Size and Chemistry of Ionic Ultramicroporous Polymers for Trace Sulfur Dioxide Capture with High Capacity and Selectivity, Angew. Chem. Int. Ed. Engl. 60 (13) (2021) 6986–6991.

[37] D. Taylor, S.J. Dalgarno, Z. Xu, F. Vilela, Conjugated porous polymers: incredibly versatile materials with far-reaching applications, Chem. Soc. Rev. 49 (12) (2020) 3981–4042.

[38] T. Skorjanc, D. Shetty, A. Trabolsi, Pollutant removal with organic macrocycle-based covalent organic polymers and frameworks, Chem 7 (4) (2021) 882–918.

[39] S. Abubakar, T. Skorjanc, D. Shetty, A. Trabolsi, Porous Polycalix[n]arenes as Environmental Pollutant Removers, ACS Appl Mater Interfaces 13 (13) (2021) 14802–14815.

[40] R. Zadmard, F. Hokmabadi, M.R. Jalali, A. Akbarzadeh, Recent progress to construct calixarene-based polymers using covalent bonds: synthesis and applications, RSC Adv. 10 (54) (2020) 32690–32722.

[41] K. Su, W. Wang, B. Li, D. Yuan, Azo-Bridged Calix[4]resorcinarene-Based Porous Organic Frameworks with Highly Efficient Enrichment of Volatile Iodine, ACS Sustainable Chem. Eng 6 (12) (2018) 17402–17409.

[42] D. An, L. Li, Z. Zhang, A.M. Asiri, K.A. Alamry, X. Zhang, Amino-bridged covalent organic Polycalix[4]arenes for ultra efficient adsorption of iodine in water, Mater. Chem. Phys. 239 (2020), 122328.

[43] D. Shetty, I. Jahovic, J. Raya, Z. Asfari, J.-C. Olsen, A. Trabolsi, Porous Polycalix[4]arenes for Fast and Efficient Removal of Organic Micropollutants from Water, ACS Appl Mater Interfaces 10 (3) (2018) 2976–2981.

[44] S. Lan, S. Zhan, J. Ding, J. Ma, D.a. Ma, Pillar[n]arene-based porous polymers for rapid pollutant removal from water, J. Mater. Chem. A 5 (6) (2017) 2514–2518.

[45] D. Shetty, I. Jahović, T. Skorjanc, T.S. Erkal, L. Ali, J. Raya, Z. Asfari, M.A. Olson, S. Kirmizialtin, A.O. Yazaydin, A. Trabolsi, Rapid and Efficient Removal of Perfluorooctanoic Acid from Water with Fluorine-Rich Calixarene-Based Porous Polymers, ACS Appl Mater Interfaces 12 (38) (2020) 43160–43166.

[46] A. Giri, M.D.W. Hussain, B. Sk, A. Patra, Connecting the Dots: Knitting C-Phenylresorcin[4]arenes with Aromatic Linkers for Task-Specific Porous Organic Polymers, Chemistry of Materials 31 (20) (2019) 8440–8450.

[47] A.A. Bhatti, M. Oguz, M. Yilmaz, Magnetizing Calixarene: Azo Dye Removal from Aqueous Media by Fe3O4 Nanoparticles Fabricated with Carboxylic-Substituted Calix[4]arene, J. Chem. Eng. Data 62 (9) (2017) 2819–2825.

[48] X. Wang, L. Xie, K. Lin, W. Ma, T. Zhao, X. Ji, M. Alyami, N.M. Khashab, H. Wang, J.L. Sessler, Calix[4]pyrrole-Crosslinked Porous Polymeric Networks for the Removal of Micropollutants from Water, Angew. Chem. Int. Ed. Engl. 60 (13) (2021) 7188–7196.

[49] H. Li, H. Huang, X. Yan, C. Liu, L. Li, A Calix[4]arene-crosslinked polymer for rapid adsorption of cationic dyes in water, Mater. Chem. Phys. 263 (2021), 124295.

[50] Y. Chen, Y. Fang, J. Yu, W. Gao, H. Zhao, X. Zhang, A silsesquioxane-porphyrin-based porous organic polymer as a highly efficient and recyclable absorbent for wastewater treatment, J. Hazard. Mater. 406 (2021), 124769.

[51] X.-C. Du, J.-H. Zhu, Z.-J. Quan, X.-C. Wang, Adsorption of rhodamine B by organic porous materials rich in nitrogen, oxygen, and sulfur heteroatoms, New J. Chem. 45 (7) (2021) 3448–3453.
[52] P. Yang, X. Hu, Y. Tu, G. Xu, L. Sun, X. Xie, The synthesis of a DMpillar[5]arene-based porous polymer with ultrafast adsorption rate and high adsorption capacity for organic micropollutants from water, Chem. Eng. J. (2021) 132418, https://doi.org/10.1016/j.cej.2021.132418.
[53] X. Yao, L. Ji, J. Guo, S. Ge, W. Lu, Y. Chen, L. Cai, Y. Wang, W. Song, An abundant porous biochar material derived from wakame (Undaria pinnatifida) with high adsorption performance for three organic dyes, Bioresour. Technol. 318 (2020), 124082.
[54] Y. Gao, S.-Q. Deng, X. Jin, S.-L. Cai, S.-R. Zheng, W.-G. Zhang, The construction of amorphous metal-organic cage-based solid for rapid dye adsorption and time-dependent dye separation from water, Chem. Eng. J. 357 (2019) 129–139.
[55] Y. Wu, Y. Liu, R. Dou, W. Tang, B. Sun, T. Gao, Z. Yang, G. Zhou, Larger pore volume tetraphenyladamantane-based hybrid porous polymers: Facile Friedel-Crafts preparation, CO_2 capture, and Rhodamine B removal properties, J. Appl. Polym. Sci. 137 (16) (2019) 48572.
[56] X. Wang, Z. Liu, F.a. Zhou, J. Huang, Imidazolium Salt-Incorporated Postcross-Linked Porous Polymers for Efficient Adsorption of Rhodamine B and Cd^{2+} from Aqueous Solution, J. Chem. Eng. Data. 65 (4) (2020) 1850–1856.
[57] H. Ma, A. Kong, Y. Ji, B. He, Y. Song, J. Li, Ultrahigh adsorption capacities for anionic and cationic dyes from wastewater using only chitosan, J. Clean. Prod. 214 (2019) 89–94.
[58] G. Yang, H. Gao, Q. Li, S. Ren, Preparation and dye adsorption properties of an oxygen-rich porous organic polymer, RSC Adv. 11 (26) (2021) 15921–15926.
[59] X. Zhao, D. Wang, C. Xiang, F. Zhang, L. Liu, X. Zhou, H. Zhang, Facile Synthesis of Boron Organic Polymers for Efficient Removal and Separation of Methylene Blue, Rhodamine B, and Rhodamine 6G, ACS. Sustain. Chem. Eng. 6 (12) (2018) 16777–16787.
[60] Y. Zhang, X. Hong, X.-M. Cao, X.-Q. Huang, B. Hu, S.-Y. Ding, H. Lin, Functional Porous Organic Polymers with Conjugated Triaryl Triazine as the Core for Superfast Adsorption Removal of Organic Dyes, ACS. Appl. Mater. Inter. 13 (5) (2021) 6359–6366.
[61] S. Wang, L. Shao, Y. Sang, J. Huang, Hollow Hyper-Cross-Linked Polymer Microspheres for Efficient Rhodamine B Adsorption and CO2 Capture, J. Chem. Eng. Data 64 (4) (2019) 1662–1670.
[62] M. Ge, H. Liu, A silsesquioxane-based thiophene-bridged hybrid nanoporous network as a highly efficient adsorbent for wastewater treatment, J. Mater. Chem. A 4 (42) (2016) 16714–16722.
[63] H. Liu, H. Liu, Selective dye adsorption and metal ion detection using multifunctional silsesquioxane-based tetraphenylethene-linked nanoporous polymers, J. Mater. Chem. A 5 (19) (2017) 9156–9162.
[64] L. Zhang, J.-S. Sun, F. Sun, P. Chen, J. Liu, G. Zhu, Facile Synthesis of Ultrastable Porous Aromatic Frameworks by Suzuki-Miyaura Coupling Reaction for Adsorption Removal of Organic Dyes, Chem. Eur. J. 25 (15) (2019) 3903–3908.
[65] R. Shen, Y. Du, X. Yang, H. Liu, Silsesquioxanes-based porous functional polymers for water purification, J. Mater. Sci 55 (17) (2020) 7518–7529.
[66] B. Wang, Z. Xie, Y. Li, Z. Yang, L. Chen, Dual-Functional Conjugated Nanoporous Polymers for Efficient Organic Pollutants Treatment in Water: A Synergistic Strategy of Adsorption and Photocatalysis, Macromolecules 51 (9) (2018) 3443–3449.
[67] A.F.M. EL-Mahdy, M.B. Zakaria, H.-X. Wang, T. Chen, Y. Yamauchi, S.-W. Kuo, Heteroporous bifluorenylidene-based covalent organic frameworks displaying exceptional dye adsorption behavior and high energy storage, J. Mater. Chem. A 8 (47) (2020) 25148–25155.
[68] H.M.H. Gad, A.A. El-Sayed, Activated carbon from agricultural by-products for the removal of Rhodamine-B from aqueous solution, J. Hazard. Mater 168 (2-3) (2009) 1070–1081.